CrossMark

ORIGINAL PAPER

Phytoplankton community responses to iron and CO_2 enrichment in different biogeochemical regions of the Southern Ocean

Hisashi Endo[1,2] · Hiroshi Hattori[3] · Tsubasa Mishima[3] · Gen Hashida[4] ·
Hiroshi Sasaki[5] · Jun Nishioka[6] · Koji Suzuki[1,2]

Abstract The ongoing rise in atmospheric CO_2 concentration is causing rapid increases in seawater $p\mathrm{CO}_2$ levels. However, little is known about the potential impacts of elevated CO_2 availability on the phytoplankton assemblages in the Southern Ocean's oceanic regions. Therefore, we conducted four incubation experiments using surface seawater collected from the subantarctic zone (SAZ) and the subpolar zone (SPZ) in the Australian sector of the Southern Ocean during the austral summer of 2011–2012. For incubations, $FeCl_3$ solutions were added to reduce iron (Fe) limitation for phytoplankton growth. Ambient and high (~ 750 µatm) CO_2 treatments were then prepared with and without addition of CO_2-saturated seawater, respectively. Non-Fe-added (control) treatments were also prepared to assess the effects of Fe enrichment (overall, control, Fe-added, and Fe-and-CO_2-added treatments). In the initial samples, the dominant phytoplankton taxa shifted with latitude from haptophytes to diatoms, likely reflecting silicate availability in the water. Under Fe-enriched conditions, increased CO_2 level significantly reduced the accumulation of biomarker pigments in haptophytes in the SAZ and AZ, whereas a significant decrease in diatom markers was only detected in the SAZ. The CO_2-related changes in phytoplankton community composition were greater in the SAZ, most likely due to the decrease in coccolithophore biomass. Our results suggest that an increase in CO_2, if it coincides with Fe enrichment, could differentially affect the phytoplankton community composition in different geographical regions of the Southern Ocean, depending on the locally dominant taxa and environmental conditions.

Keywords Ocean acidification · Iron · Southern Ocean · Phytoplankton community composition · Diatoms · Haptophytes

✉ Hisashi Endo
endo@scl.kyoto-u.ac.jp

✉ Koji Suzuki
kojis@ees.hokudai.ac.jp

[1] Faculty of Environmental Earth Science, Hokkaido University, North 10 West 5, Kita-ku, Sapporo, Hokkaido 060-0810, Japan

[2] CREST, Japan Science and Technology, North 10 West 5, Kita-ku, Sapporo, Hokkaido 060-0810, Japan

[3] Department of Marine Biology and Sciences, Tokai University, Minamisawa, Minami-ku, Sapporo, Hokkaido 005-8601, Japan

[4] National Institute of Polar Research, 10-3 Midori-cho, Tachikawa, Tokyo 190-8518, Japan

[5] Department of Biological Sciences, Ishinomaki Senshu University, Shinmito Minamisakai, Ishinomaki, Miyagi 986-8580, Japan

[6] Pan-Okhotsk Research Center, Institute of Low Temperature Science, Hokkaido University, North 19 West 8, Kita-ku, Sapporo 060-0819, Japan

Introduction

The atmospheric CO_2 concentration has increased from approximately 270 ppm in preindustrial times to >400 ppm in 2016 (NOAA 2016) as a result of human activity. Absorption of anthropogenic CO_2 is causing an increase in seawater $p\mathrm{CO}_2$ levels and a decrease in pH (i.e., ocean acidification, OA) (Caldeira and Wickett 2003). It is widely accepted that OA can both positively

and negatively affect marine organisms; For example, previous studies have demonstrated that OA can reduce calcium carbonate ($CaCO_3$) skeleton formation in a wide variety of organisms because of decreased carbonate saturation (Riebesell et al. 2000; Comeau et al. 2009; Moy et al. 2009). Because the reduction in $CaCO_3$ saturation is more pronounced in cold, high-latitude areas such as the Southern Ocean (Orr et al. 2005), calcifying organisms such as pteropods (Bednaršek et al. 2012) and coccolithophores (Freeman and Lovenduski 2015) may be particularly affected in these areas.

The Southern Ocean comprises approximately 20% of the world's ocean and is responsible for nearly half of global anthropogenic CO_2 uptake (Khatiwala et al. 2009; Takahashi et al. 2012). Although phytoplankton play pivotal roles in sustaining biogeochemical cycles and marine ecosystems in the Southern Ocean (Marx and Uhen 2010), the contribution of primary productivity to atmospheric CO_2 sequestration is thought to be relatively low in oceanic regions (Huntley et al. 1991; Arrigo et al. 2008). A main cause of this low productivity is the relatively low availability of iron (Fe) in surface seawater; the Southern Ocean oceanic region is generally classified as a high-nitrate, low-chlorophyll (HNLC) region (Martin et al. 1990; de Baar et al. 1995; Coale et al. 2004). Atmospheric dust deposition is a major Fe source in the Southern Ocean, and potentially drives phytoplankton blooms in this region (Bowie et al. 2009). A previous climate modeling study suggested that dust supply to the surface of the Southern Ocean could increase more than tenfold from 2000 to 2100, as a result of desiccation and changes in vegetation on the Australian continent (Woodward et al. 2005). Additionally, Fe input from icebergs and sea-ice to the surface water will likely increase in the future as a result of climate change (Boyd et al. 2012; Hutchins and Boyd 2016). Therefore, Fe limitation in the Southern Ocean may be mitigated to some extent in the future.

Another remarkable characteristic of the Southern Ocean is the presence of several oceanic fronts (Fig. 1), which separate distinct water masses (Orsi et al. 1995; Longhurst 2007). These divide the Southern Ocean into distinct oceanic regions with different physical and chemical properties (Longhurst 2007). Additionally, because surface water flows northward across the polar and subarctic fronts (Speer et al. 2000), a large latitudinal gradient of nutrients in the euphotic layer occurs from south to north of these fronts (Coale et al. 2004; Takao et al. 2014). Consequently, there are clear gradients in phytoplankton community composition from siliceous diatoms in the southern to nonsiliceous phytoplankton groups (e.g., haptophytes and dinoflagellates) in the northern Southern Ocean (Ishikawa et al. 2002; Takao et al. 2014; Malinverno et al. 2016).
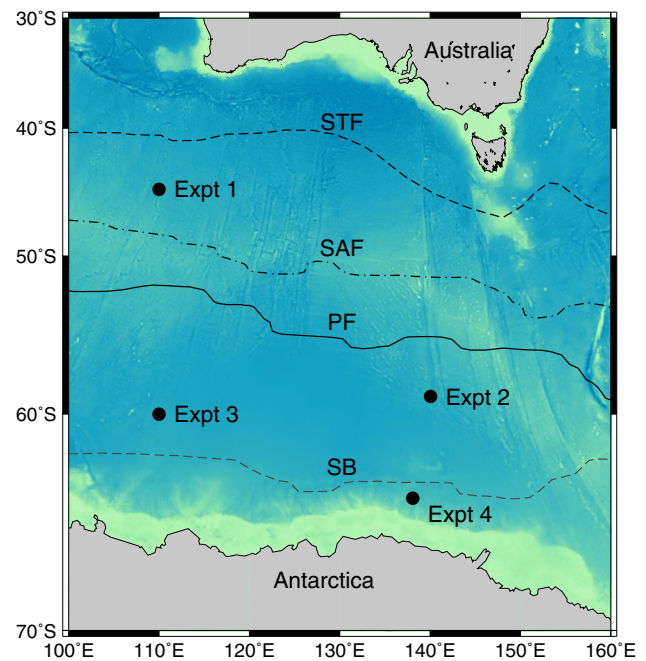

Fig. 1 Incubation experiment sampling sites. *Each line* indicates the climatological location of four fronts defined by Orsi et al. (1995): *STF* subtropical front, *SAF* subarctic front, *PF* polar front, *SB* southern boundary of the Antarctic Circumpolar Current. The frontal data were obtained from the World Ocean Circulation Experiment (WOCE) Southern Ocean Atlas Database

Laboratory incubation experiments have suggested that the sensitivity of Antarctic phytoplankton to increased CO_2 levels varies among species and with environmental conditions (Trimborn et al. 2013, 2014; Xu et al. 2014). Moreover, high CO_2 conditions might change the competitive relationships between phytoplankton species (Trimborn et al. 2013). Therefore, the impact of OA would differ among geographical regions in the Southern Ocean, reflecting the phytoplankton community characteristics and the limiting nutrients. In fact, some experiments have demonstrated that changes in phytoplankton community composition and/or primary productivity under elevated CO_2 treatments in the Southern Ocean are possible (Tortell et al. 2008; Feng et al. 2010; Hoppe et al. 2013; Maas et al. 2013). However, these studies have only been conducted in high-latitude areas (e.g., the Ross and Weddell Seas). At present, there are no reports on the potential impact of OA on phytoplankton assemblages in middle- and low-latitude regions of the Southern Ocean.

Therefore, we conducted CO_2-manipulated bottle incubation experiments in four distinct Southern Ocean oceanic regions to assess the responses of marine phytoplankton assemblages to high CO_2 levels under Fe-replete conditions. We primarily focused on geographical differences in CO_2-induced community composition changes, as estimated from pigment signatures and microscopic analysis.

Phytoplankton photosynthetic physiology was also assessed using the maximum photochemical quantum efficiency (F_v/F_m) of photosystem II, diatom-specific *rbcL* gene transcriptional activity, and photosynthesis–irradiance (P–E) parameters.

Materials and methods

Experimental setup

This study was carried out aboard the RT/V *Umitaka-Maru* (Tokyo University of Marine Science and Technology) during the UM-11-7 cruise in the austral summer of December 2011 to January 2012. Four incubation experiments were conducted using seawater collected from different stations located in the subantarctic zone (SAZ, station C02), the Antarctic zone (AZ, stations C07 and D13), and the subpolar zone (SPZ, station D07) in the Australian sector of the Southern Ocean (Fig. 1; Table 1). Trace-metal-clean seawater samples were collected at approximately 15 m depth at stations C02 (45°00′S, 110°00′E, 30 December, 2011), C07 (60°00′S, 110°00′E, 3 January, 2012), D07 (64°21′S, 138°05′E, 22 January, 2012), and D13 (59°00′S, 140°03′E, 27 January, 2012) (Fig. 1) using an acid-clean Teflon® pump system (model PFD, Asti Co.). Average daytime photosynthetic active radiation (PAR) in the air ranged from 211 to 857 μmol photons m^{-2} s^{-1}; these values largely depended on the weather conditions on each sampling date (Online Resource 1).

Trace-metal-clean methods were employed for sampling, and all of the plastic implements for the incubation study were acid cleaned according to Takeda and Obata (1995). In each experiment, eight 9-L polycarbonate bottles (Nalgene) were filled with seawater through silicon tubing with a 250-μm-mesh Teflon® net to remove large plankton. Two bottles were used to obtain samples for the initial conditions. Another two bottles were unchanged and were used as control treatments. FeCl₃ solutions (5 nM final concentration) were added to the remaining four bottles to reduce Fe limitation for microbial assemblages. The high-CO_2 treatment (i.e., 750 μatm) was created by addition of CO_2-saturated seawater, which was prepared by pumping pure CO_2 gas into ambient seawater, in two of the four Fe-added bottles. The non-Fe-added (control), Fe-added (Fe), and Fe-and-CO_2-added (Fe+C) treatments were prepared in duplicate. We did not add any macronutrients to the treatments. The experiments conducted at stations C02, D13, C07, and D07 are named Expt 1, Expt 2, Expt 3, and Expt 4, respectively. After adjusting the Fe and pCO₂ levels, all of the bottles were incubated for 2.9–4.0 days in a laboratory incubator (MIR-554, Sanyo) adjusted to ambient temperature. The irradiance level was set at 100 μmol photons m^{-2} s^{-1} using fluorescent lamps (Plantlux, Toshiba). Light–dark cycles in the incubator were also adjusted to the in situ conditions at the sampling stations. A detailed description of the incubation conditions is given in Table 2. The samples for all treatments were collected between 5:00 and 6:00 a.m. local time at the end of the incubations.

Carbonate chemistry, nutrients, and iron analysis

The total alkalinity (TA) and dissolved inorganic carbon (DIC) samples were collected in gastight glass vials, and HgCl₂ was added prior to storage at 4 °C to await analysis. The nutrient samples were collected in plastic tubes and stored at −20 °C until analysis. The samples taken for measurement of total dissolvable Fe (TDFe, unfiltered) at the beginning of the experiment were collected directly from the clean pump system, adjusted to pH <1.8 by adding 20% HCl (Tamapure AA-10, Tama Chemicals), and stored at room temperature until analysis.

The TA and DIC samples were measured according to the method of Edmond (1970). Titration analysis stability was verified using DIC reference material (KANSO), for which the DIC value was traceable to the certified reference material supplied by Andrew Dickson at the University of California, San Diego. Seawater pCO₂ and pH levels were calculated using CO2SYS Excel Macro (Pierrot et al. 2006). Nitrate + nitrite (NO₃ + NO₂), nitrite (NO₂),

Table 1 Locations and hydrographical conditions at each sampling site

Expt	Lat (S)	Long (E)	Temp (°C)	Sal	NO₃ (μmol L⁻¹)	NO₂ (μmol L⁻¹)	PO₄ (μmol L⁻¹)	Si(OH)₄ (μmol L⁻¹)	TDFe (μmol L⁻¹)
1	45°00′	110°00′	10.5	34.42	10.75	0.22	0.76	0.74	0.851
2	59°00′	140°03′	3.62	33.81	24.96	0.21	1.59	11.11	0.043
3	60°00′	110°00′	2.38	33.62	25.82	0.25	1.61	29.54	0.052
4	64°21′	138°05′	0.89	33.72	25.70	0.30	1.65	39.75	0.024

Lat latitude, *Long* longitude, *Temp* temperature, *Sal* salinity, *NO₃* nitrate, *NO₂* nitrite, *PO₄* phosphate; *Si(OH)₄* silicate, *TDFe* total dissolvable iron

Table 2 Incubation conditions in each experiment

Expt	Time (days)	(°C)	Photon flux (μmol m^{-1} s^{-1})	L:D cycle (h:h)	Light on (local time)	Light off (local time)	Injection of CO_2-saturated seawater (mL L^{-1})
1	2.9	10.5	100	15.5:8.5	5:00	20:30	2.5
2	3.3	3.6	100	17.0:7.0	4:30	21:30	1.8
3	3.7	2.5	100	18.5:5.5	3:30	22:00	1.6
4	4.0	1.0	100	19.25:4.75	3:15	22:30	1.4

phosphate (PO_4), and silicate [$Si(OH)_4$] concentrations were determined using a segmented continuous flow analyzer (QuAAtro-2, BL-Tec). Total TDFe concentrations were measured by flow-injection method with chemiluminescence detection (Obata et al. 1997).

HPLC and CHEMTAX analysis

High-performance liquid chromatography (HPLC) was used to determine phytoplankton pigment concentrations following Endo et al. (2013). HPLC pigment analysis samples (600–1000 mL) were filtered through GF/F filters under gentle vacuum (<0.013 MPa) and stored in either liquid nitrogen or a deep freezer (−80 °C) until analysis.

To estimate the class-level phytoplankton community composition, the CHEMTAX program based on the HPLC pigment analysis was used according to Endo et al. (2013). The program obtained the optimal initial ratios according to the method of Latasa (2007). In this study, the initial pigment ratios were obtained from Wright and van den Enden (2000), who investigated phytoplankton community compositions in the Southern Ocean. The initial and final (optimal) pigment matrices are shown in Online Resources 2 and 3, respectively.

SEM analysis

Scanning electron microscopy (SEM) samples were fixed with 20% neutral buffered formalin solution (1% final concentration) adjusted to pH 8.1 using 0.1 M NaOH and then stored at 4 °C until analysis. The samples (30–50 mL) were then filtered onto a polycarbonate filter (Nuclepore, 2.0 μm pore size) using a 5-mm-diameter glass funnel, dried at 60 °C for 24 h, and sputter-coated with platinum:palladium (80:20) using an ion sputtering coater (JFC-1100E, JEOL). SEM images were obtained using a JMS-840A scanning microscope (JEOL). Phytoplankton cell identification (particularly diatoms and haptophytes) was conducted following Thomas (1997), Young et al. (2003), and Scott and Thomas (2005). Cell counts were conducted for a whole to one-quarter of the filtered area (diameter 5 mm).

FIRe fluorometry

Fluorescence induction and relaxation (FIRe) fluorometry seawater samples were initially incubated in a dark incubator for 30 min to open the phytoplankton photosystem II (PSII) reaction centers. F_v/F_m values were measured using a FIRe fluorometer (Satlantic) following the method of Takao et al. (2014).

qPCR and qRT-PCR

DNA samples (600–1000 mL) were collected on 0.2-μm pore size polycarbonate Nuclepore^{TM} filters (Whatman) with gentle vacuum and stored in either liquid nitrogen or a deep freezer at −80 °C until analysis. For RNA analysis, seawater samples (600–1000 mL) were also filtered onto 0.2-μm pore size polycarbonate Nuclepore^{TM} filters (Whatman). The filters were stored in 1.5-mL cryotubes filled with 0.2 g muffled 0.1-mm glass beads and 600-μL RLT buffer (Qiagen) with 10 μL mL^{-1} β-mercaptoethanol (Sigma, USA). The RNA samples were stored in either liquid nitrogen or a deep freezer at −80 °C until analysis. The diatom-specific *rbcL* gene, which encodes the large subunit of the CO_2-fixing enzyme ribulose 1,5-bisphosphate carboxylase/oxygenase (RuBisCO), and its transcript were quantified by quantitative polymerase chain reaction (qPCR) and quantitative reverse-transcription polymerase chain reaction (qRT-PCR), respectively, following Endo et al. (2015). Diatom-specific *rbcL* transcriptional activity was then calculated as transcript abundance normalized to gene abundance (cDNA/DNA).

Photosynthesis–irradiance (P–E) curve experiments

P–E curve experiments were performed before and after the incubation experiments. At the end of the incubation experiments, P–E curves were obtained in the following sequence: control (5:00–7:00 a.m.), Fe (7:00–9:00 a.m.), and Fe+C treatments (9:00–11:00 a.m.). The P–E curve experiment was conducted on a single sample for each treatment. First, seawater samples were immediately dispensed into 275-mL acid-clean polystyrene bottles and

inoculated with NaH^{13}CO$_3$ solution (99 atm.% ^{13}C, Shoko), which was equivalent to ~10% DIC in the seawater. Duplicate water samples were filtered onto precombusted Whatman GF/F filters (25 mm diameter) under gentle vacuum (<100 mmHg) immediately after adding the NaH^{13}CO$_3$. The samples were then incubated for 2 h at ambient temperature (Isada et al. 2009) with a 150-W metal halide lamp (HQI-T 150 W/WDL/UVS, Mitsubishi/Osram) as light source. Irradiance levels in the incubation bottles ranged between 7 and 1774 μmol photons m^{-2} s^{-1}. After incubation, the samples were filtered in the same manner. The filters were then immediately stored in either liquid nitrogen or a deep freezer (−80 °C) until analysis.

Once thawed, the filters were exposed to HCl fumes to remove inorganic carbon and then completely dried in a desiccator under vacuum for >24 h. The particulate organic carbon (POC) and ^{13}C abundance in the samples were determined using a mass spectrometer (Delta V plus, Thermo Fisher Scientific Inc.) with inline elemental analyzer (Flash EA1112, Thermo Fisher Scientific Inc.). Photosynthetic rates based on the ^{13}C tracer technique were determined following the method of Hama et al. (1983). The P–E curve parameters were obtained using the photoinhibition model of Platt et al. (1980). Detailed procedures for the P–E curve experiment are described in Takao et al. (2014).

Statistical analysis

One-way analysis of variance (ANOVA) was used to examine the differences among the three treatments. Tukey's post hoc test was also used to identify paired differences between mean values. The effects of Fe enrichment were assessed by comparisons between the control and Fe-added treatments. Similarly, the effects of CO$_2$ enrichment were assessed by comparisons between the Fe-added and Fe-and-CO$_2$-added treatments. Values of $p < 0.05$ were considered statistically significant.

The characteristics of the phytoplankton community composition based on CHEMTAX were evaluated by principal component analysis (PCA) in R (https://www.r-project.org/). To compare the magnitude of the effects of Fe and CO$_2$ enrichment on the CHEMTAX-based taxonomic composition among the experiments, we used Euclidean distance as a dissimilarity measure between the control versus Fe and Fe versus Fe+CO$_2$ treatments for each experiment.

Results

Carbonate chemistry, nutrients, and iron

The initial seawater TA concentrations were 2313.9, 2278.1, 2292.6, and 2244.6 μmol kg^{-1} in Expts 1, 2, 3, and

4, respectively (Table 3). These values did not change substantially during incubation. The initial DIC concentrations were 2110.4, 2139.4, 2156.6, and 2126.4 μmol kg^{-1} in Expts 1, 2, 3, and 4, respectively. Addition of CO$_2$-saturated seawater to each sample led to significant changes in seawater DIC, pCO$_2$, and pH levels, which remained until the end of the experiments (Table 3). The method used to control seawater pCO$_2$ in this study succeeded in creating the intended values (i.e., ~ 750 μatm) without significant variations between duplicate bottles.

The macronutrient concentrations were consistently high in Expts 2, 3, and 4 but relatively low in Expt 1 (Table 1). However, the TDFe concentrations in Expts 2, 3, and 4 were relatively low, but those in Expt 1 were relatively high (Table 1). Because our incubation periods were consistently short, the macronutrient concentrations remained largely unchanged during all of the incubations (Online Resource 4).

Phytoplankton pigments

The initial Chl-a concentrations in Expts 1, 2, 3, and 4 were 0.26 ± 0.01, 0.34 ± 0.03, 0.62 ± 0.00, and 0.29 ± 0.01 μg L^{-1}, respectively. In Expts 1, 2, and 3, the Chl-a concentration increased significantly in the Fe compared with the control treatments (ANOVA and Tukey's test, $p < 0.05$), while no significant effect was observed in Expt 4 (Fig. 2; Table 4). After incubation, the Chl-a concentration was significantly lower in the high-CO$_2$ treatment than that in the ambient CO$_2$ treatment in the Fe samples in Expt 3 (ANOVA and Tukey's test, $p < 0.05$), while no significant CO$_2$ effect was detected in the other experiments (Fig. 2).

The carotenoid 19′-hexanoyloxyfucoxanthin (19′-Hex), a haptophyte biomarker (Jeffrey and Wright 1994), was an abundant component of the pigment array in the initial sample in Expt 1 (Fig. 2). In contrast, fucoxanthin (Fuco), which is mainly derived from oceanic diatoms (Ondrusek et al. 1991), was the most abundant pigment in the initial samples in Expts 2, 3, and 4 (Fig. 2). Although Fuco is also a major haptophyte pigment (Jeffrey and Vesk. 1997), a significant positive correlation was detected between diatom-derived Chl-a estimated by CHEMTAX analysis and Fuco concentration estimated by HPLC in our experiments ($r^2 = 0.972$, $p < 0.01$; Online Resource 5). Thus, we used the Fuco pigment as an indicator of diatom biomass.

After incubation, the Fuco concentration was significantly higher in the Fe treatments than in the controls in Expt 2 and 3 (ANOVA and Tukey's test, $p < 0.05$; Table 4). Additionally, the Fuco concentration in the Fe+C treatment was significantly lower than that in the Fe treatment in Expt 3 (ANOVA and Tukey's test, $p < 0.05$). Significant differences among treatments were also

Table 3 Carbonate chemistry (value ± 1SD, $n = 2$, except for initial, n = 1) at the beginning and end of each incubation experiment

Expt		TA (µmol kg^{-1})	DIC (µmol kg^{-1})	pCO$_2$ (µatm)	pH (total)
1	Int	2313.9	2110.4	376.7	8.08
	Int+C	2289.2	2194.7	749.5	7.81
	Control	2301.1 ± 16.7	2100.0 ± 13.4	377.3 ± 2.3	8.08 ± 0.01
	Fe	2304.8 ± 5.5	2094.9 ± 2.7	361.0 ± 4.1	8.09 ± 0.01
	Fe+C	2341.8 ± 25.7	2226.4 ± 24.7	667.7 ± 6.2	7.86 ± 0.00
2	Int	2278.1	2139.4	395.9	8.04
	Int+C	2281.6	2227.5	748.9	7.79
	Control	2278.2 ± 0.4	2137.6 ± 1.2	390.8 ± 4.3	8.05 ± 0.00
	Fe	2280.8 ± 2.1	2139.0 ± 2.4	388.5 ± 1.1	8.05 ± 0.00
	Fe+C	2276.5 ± 1.4	2215.4 ± 0.7	708.3 ± 4.1	7.81 ± 0.00
3	Int	2292.6	2156.6	379.4	8.06
	Int+C	2289.8	2243.9	753.4	7.78
	Control	2315.8 ± 9.3	2175.2 ± 7.5	376.1 ± 2.2	8.07 ± 0.00
	Fe	2320.0 ± 6.9	2171.8 ± 6.8	359.0 ± 1.4	8.08 ± 0.00
	Fe+C	2327.9 ± 6.1	2262.3 ± 11.4	658.3 ± 30.2	7.85 ± 0.02
4	Int	2244.6	2126.4	403.4	8.02
	Int+C	2251.2	2201.8	695.4	7.80
	Control	2245.3 ± 3.1	2119.6 ± 2.8	384.4 ± 0.1	8.04 ± 0.00
	Fe	2248.2 ± 1.8	2119.2 ± 2.5	376.0 ± 2.3	8.05 ± 0.00
	Fe+C	2247.2 ± 3.1	2190.6 ± 2.5	656.5 ± 2.8	7.83 ± 0.00

Int initial, *Int+C* initial with added CO$_2$-saturated seawater, *Fe* Fe-added, *Fe+C* Fe-and-CO$_2$-added

detected with respect to 19′-Hex concentrations (ANOVA, $p < 0.05$). The values were significantly higher in the Fe treatments than in the controls in Expts 1, 2, and 3, while the reverse effect was observed in Expt 4 (Tukey's test, $p < 0.05$, Table 4). The 19′-Hex concentration values were significantly lower in the Fe+C than in the Fe treatments in Expts 1 and 2 (Tukey's test, $p < 0.05$).

CHEMTAX outputs

In our experiments, the initial phytoplankton assemblages were dominated by either diatoms or haptophytes (Fig. 3). Haptophyte type 4, which mainly consists of noncalcifying groups, such as *Phaeocystis* spp. (Jeffrey and Wright 1994), was the prevailing group in Expt 1 with a mean Chl-*a* biomass contribution of 56%, the proportions of which decreased with latitude (40, 21, and 6% in Expts 2, 3, and 4, respectively). Haptophyte type 3, which comprises calcifying coccolithophores (Jeffrey and Wright 1994), also made an important contribution to the initial phytoplankton assemblage in Expt 1 (14%). Diatoms were a minor component of the initial phytoplankton community in Expt 1 (5%), but their contribution increased southward (56, 71, and 76% in Expts 2, 3, and 4, respectively).

After incubation, diatom contributions were significantly higher in the Fe than in the control treatments in Expts 2–4 (ANOVA and Tukey's test, $p < 0.05$), whereas no significant difference was detected in Expt 1 (Fig. 3; Table 4). No significant difference was observed in the contribution of diatoms to the Chl-*a* biomass between the ambient- and high-CO$_2$ treatments under the Fe-added conditions. The contributions of haptophyte type 3 to the Chl-*a* biomass were significantly higher in the Fe than in the control treatments in Expt 1 (ANOVA and Tukey's test, $p < 0.05$), while the reverse effect was observed in Expt 4 (control > Fe, Tukey's test, $p < 0.05$). A significant difference was also detected between the Fe and Fe+C treatments in Expt 1, and the value was higher under ambient than under high CO$_2$ levels (Tukey's test, $p < 0.05$). The relative contributions of haptophyte type 4 were lower in the Fe than in the control treatments in Expts 1, 2, and 3 (ANOVA and Tukey's test, $p < 0.05$), whereas a small and insignificant difference was observed in Expt 4. The contributions of haptophyte type 4 did not differ significantly between the Fe and Fe+C treatments, except in Expt 1, where they were higher in the high CO$_2$ compared with the ambient CO$_2$ treatment (ANOVA and Tukey's test, $p < 0.05$).

In the PCA ordination, the CHEMTAX-based phytoplankton communities were clearly separated from each other in the four experiments (Fig. 4a). The first and second axes explained 80.1 and 9.6% of the total community

Fig. 2 **a** Chl *a*, **b** Fuco, and **c** 19′-hex concentrations on initial and final sampling days. Int, Ctrl, Fe, and Fe+C indicate initial, control, Fe-added, and Fe-and-CO_2-added treatments, respectively. All data are the average of duplicate samples, and error bars represent ±1SD between replicates
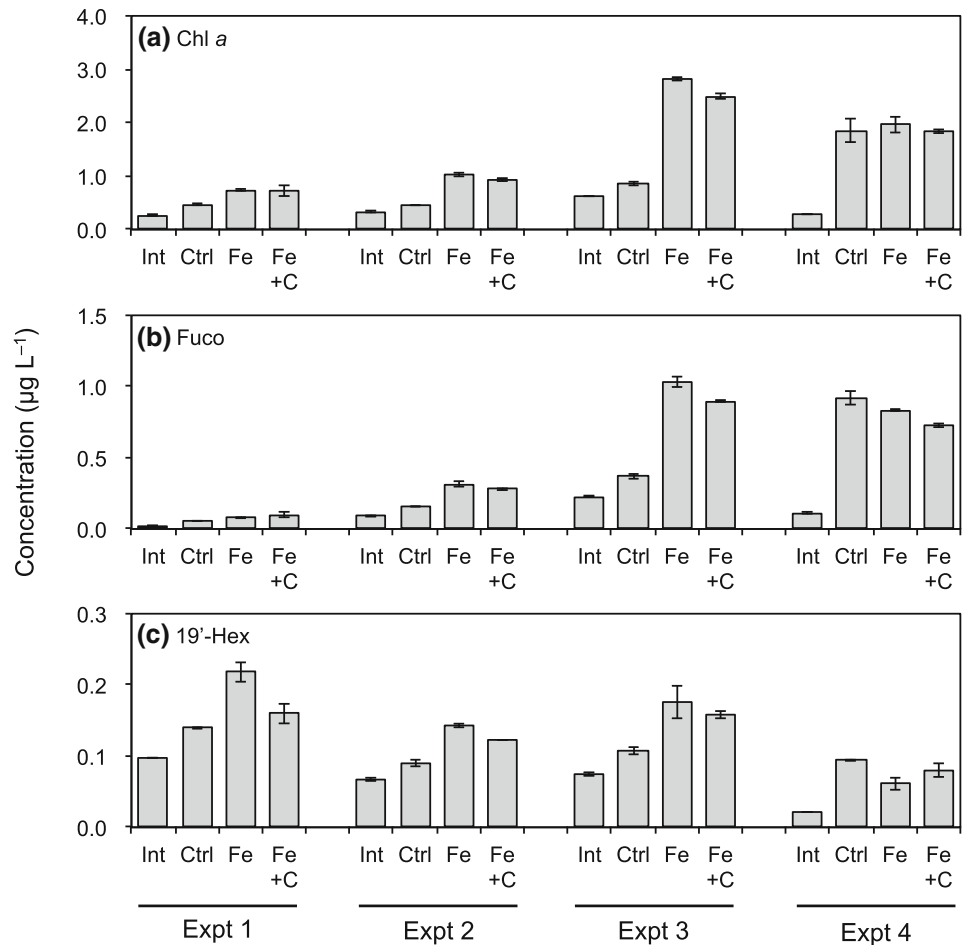

Table 4 List of *p* values obtained from ANOVA with Tukey's multiple comparison tests. Values of $p > 0.05$ are not shown

Expt		Chl *a*	Fuco	19′-Hex	Diatoms	Hapto3	Hapto4	F_v/F_m	*rbcL* copy
1	Ctrl versus Fe	0.043		0.013		0.012	0.003	<0.001	
	Fe versus Fe+C			0.030		0.009	0.032		
2	Ctrl versus Fe	<0.001	0.002	<0.001	0.030		0.022	<0.001	
	Fe versus Fe+C			0.012					
3	Ctrl versus Fe	<0.001	<0.001	0.034	0.002		0.006	<0.001	
	Fe versus Fe+C	0.011	0.018					0.036	
4	Ctrl versus Fe			0.038	0.095	0.019		0.025	
	Fe versus Fe+C								

Abbreviations: as in Figs. 2 and 3

composition variability, respectively. Based on the CHEMTAX-based community composition Euclidean distances, the difference between the control and Fe-added treatments was the highest in Expt 1, followed by Expts 2, 3, and 4 (Fig. 4b). The differences in community composition between the ambient- and high-CO_2 treatments were also the highest in Expt 1, whereas the differences were relatively low in Expts 2, 3, and 4 (Fig. 4c).

SEM observation

Microscopic observation identified 24 diatom and 13 haptophyte species (Hattori et al. in prep.). Haptophyte abundance exceeded that of diatoms in the initial samples in all of the experiments (Table 5). The initial diatom cell abundances were higher at the stations in the AZ (Expts 2 and 3; $2.3–10.2 \times 10^3$ cells L^{-1}) than those in the SPZ
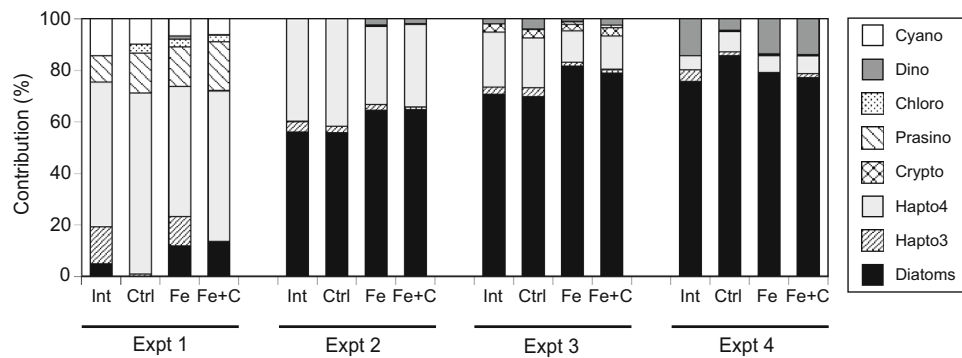
Fig. 3 Mean contributions of each phytoplankton group to total Chl-a biomass as estimated by CHEMTAX analysis. Int, Ctrl, Fe, and Fe+C indicate initial, control, Fe-added, and Fe-and-CO_2-added treatments, respectively. Data are the average of duplicate samples.

Hapto3 haptophytes type 3, *Hapto4* haptophytes type 4, *Crypto* cryptophytes, *Prasino* prasinophytes, *Chloro* chlorophytes, *Dino* dinoflagellates, *Cyano* cyanobacteria. Haptophytes types 3 and 4 mainly consist of coccolithophores and *Phaeocystis* spp., respectively

Fig. 4 a Principal component analysis (PCA) ordination incorporating phytoplankton taxa relative contributions (estimated from CHEMTAX analysis). Dissimilarity (Euclidean distance) of CHEMTAX-based community composition (%) between **b** control and Fe treatments and **c** between Fe and Fe+CO_2 treatments. Int, Ctrl, Fe, and Fe+C indicate initial, control, Fe-added, and Fe-and-CO_2-added treatments, respectively. Note that the distances in **b** and **c** are not derived from the PCA ordination, but from the overall community composition
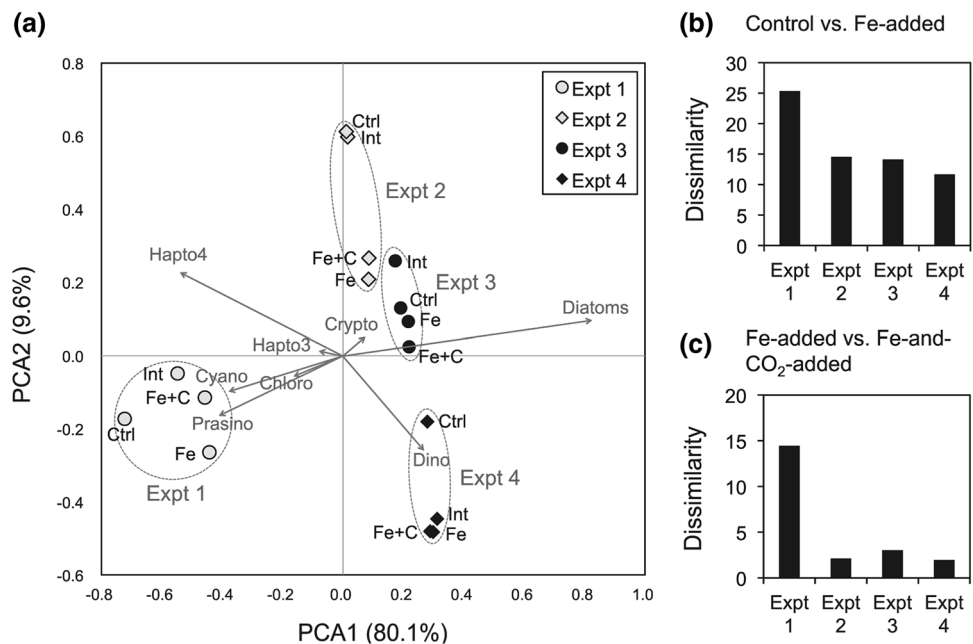
(Expt 4; 1.1×10^3 cells L^{-1}). Among the diatom community, the pennate diatom *Fragilariopsis kerguelensis* was the most abundant in Expts 2 and 3, whereas the centric diatom *Chaetoceros* sp. dominated in Expt 4. Diatom abundance was very low in the experiment conducted in the SAZ (Expt 1; 40.0 cells L^{-1}). The noncalcifying *Phaeocystis antarctica* was dominant in the haptophyte community ($1.0–2.6 \times 10^5$ cells L^{-1}) in all of the initial samples, while the coccolithophore *Emiliania huxleyi* morphotype B/C was also abundant (2.5×10^4 cells L^{-1}) in Expt 2. After incubation, both diatom and haptophyte cell abundances were higher in the Fe than those in the control treatments. Furthermore, both diatom and haptophyte cell abundances were higher in the Fe than in the Fe+C treatment.

Maximum quantum efficiency of PSII

The F_v/F_m values in the initial samples were 0.21 ± 0.02, 0.15 ± 0.01, 0.19 ± 0.01, and 0.28 ± 0.02 in Expts 1, 2, 3, and 4, respectively (Fig. 5a). After incubation, the F_v/F_m values in the Fe treatments were significantly higher than those in the control treatments in all of the experiments (ANOVA and Tukey's test, $p < 0.05$). However, a CO_2-related change in F_v/F_m was only detected in Expt 3 (Fe+C < Fe, Tukey's test, $p < 0.05$).

Diatom-specific *rbcL* transcription

The initial transcript abundance values of the diatom-specific *rbcL* normalized to gene abundance (*rbcL* cDNA/

Table 5 Diatom and haptophyte cell abundances ($\times 10^3$ cells L^{-1}) estimated by SEM analysis

Expt		Diatom total	Coccolithophore total	*Phaeocystis antarctica*
1	Initial	0.04	3.67	104.52
	Control	0.02	40.53	93.59
	Fe	0.07	98.24	161.45
	Fe+C	0.00	20.74	81.99
2	Initial	2.32	25.52	110.16
	Control	2.90	27.68	184.48
	Fe	7.63	86.32	505.42
	Fe+C	4.50	18.33	126.79
3	Initial	10.22	0.20	145.88
	Control	14.08	3.36	159.52
	Fe	49.90	36.00	303.44
	Fe+C	26.73	25.66	202.25
4	Initial	1.10	0.00	225.28
	Control	2.30	0.00	230.92
	Fe	3.67	0.00	496.15
	Fe+C	2.73	0.00	325.30

Fig. 5 **a** Maximum photochemical quantum efficiency (F_v/F_m), **b** *rbcL* cDNA abundance normalized to its gene copy number (cDNA/DNA), and **c** Chl-*a* normalized maximum photosynthetic rate (P_{max}^B). Int, Ctrl, Fe, and Fe+C indicate initial, control, Fe-added, and Fe-and-CO_2-added treatments, respectively. Data are the average of duplicate samples, except for P_{max}^B, which was estimated from a single sample. Error bars represent ± 1 SD
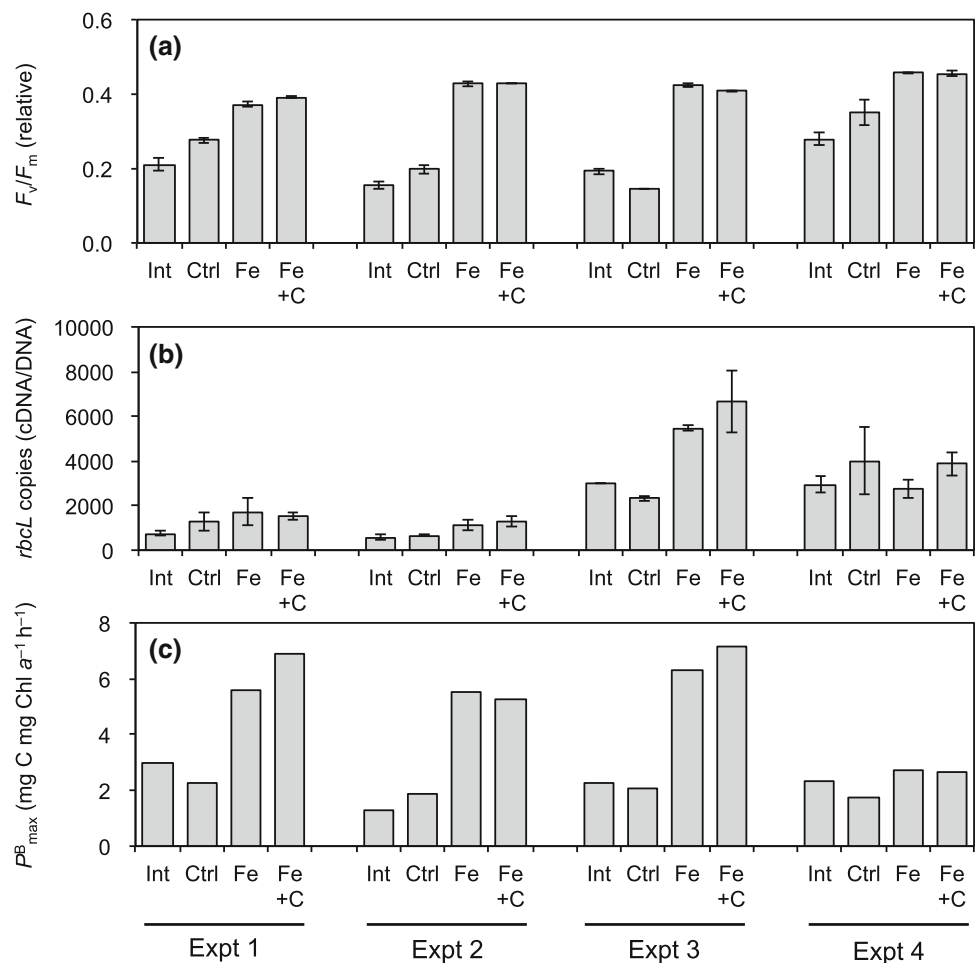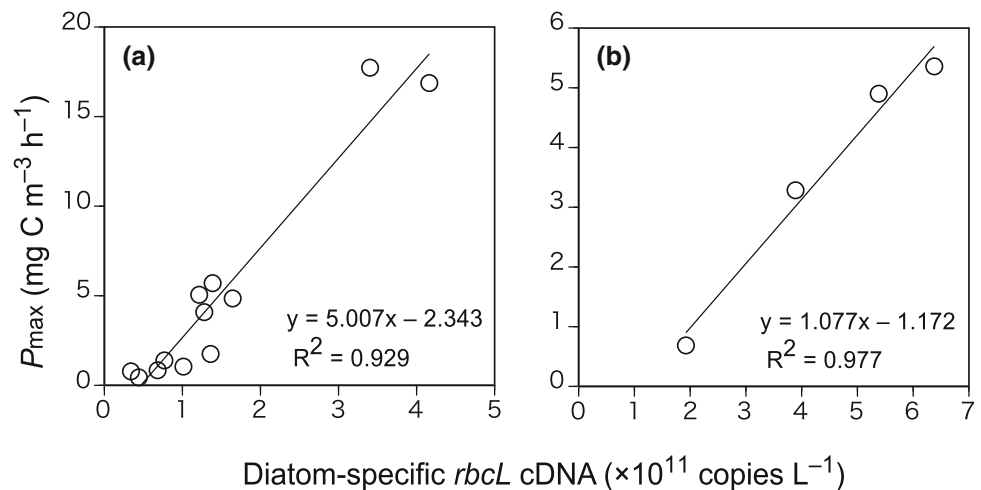
Table 6 Photosynthesis–irradiance (P–E) parameters at the beginning and end of each incubation experiment

Expt		α^B ([mg C (mg Chl-a)$^{-1}$ h^{-1}] (μmol photons m^{-2} s^{-1})$^{-1}$)	P^B_{max} (mg C (mg Chl-a)$^{-1}$ h^{-1})	P_{max} (mg C m^{-3} h^{-1})	E_k (μmol photons m^{-2} s^{-1})
1	Initial	0.030	2.95	0.78	97.2
	Control	0.030	2.26	1.04	75.2
	Fe	0.064	5.59	4.08	87.3
	Fe+C	0.085	6.92	5.05	81.6
2	Initial	0.025	1.31	0.44	52.3
	Control	0.024	1.90	0.84	78.2
	Fe	0.089	5.55	5.70	62.7
	Fe+C	0.033	5.24	4.85	157.4
3	Initial	0.028	2.25	1.39	79.8
	Control	0.026	2.04	1.75	77.3
	Fe	0.120	6.33	16.87	52.6
	Fe+C	0.133	7.12	17.73	53.4
4	Initial	0.029	2.35	0.69	80.4
	Control	0.036	1.77	3.28	49.6
	Fe	0.046	2.73	5.36	59.0
	Fe+C	0.053	2.66	4.90	50.3

α^B initial slope of the P–E curve; P^B_{max} light-saturated maximum photosynthetic rate normalized to Chl-a, P_{max} light-saturated maximum photosynthetic rate, E_k light saturation index defined by P^B_{max} and α^B (i.e., P^B_{max}/α^B)

Fig. 6 Relationships between maximum photosynthetic rate (P_{max}) and diatom-specific *rbcL* gene transcript abundance during **a** Expts 1, 2, and 3 ($n = 12$), and **b** Expt 4 ($n = 4$)

(a) y = 5.007x − 2.343
R^2 = 0.929

(b) y = 1.077x − 1.172
R^2 = 0.977

P_{max} (mg C m^{-3} h^{-1})

Diatom-specific *rbcL* cDNA ($\times 10^{11}$ copies L^{-1})

DNA) were higher in Expts 3 and 4 than in Expts 1 and 2 (Fig. 5b). After incubation, the *rbcL* cDNA/DNA values did not differ significantly among the treatments in any of the experiments (ANOVA, $p > 0.05$).

P–E parameters

In Expts 1, 2, and 3, the Chl-*a* normalized light-saturated maximum photosynthetic rates (P^B_{max}) were remarkably higher in the Fe-added treatment than in the control treatment, but the minimal difference was found in Expt 4

(Fig. 5c; Table 6). CO_2 enrichment did not affect P^B_{max}. The α^B values were consistently higher in the Fe than in the control treatments in all of the experiments, whereas no consistent trend was observed between the Fe and Fe+C treatments (Table 6). The E_k values did not differ significantly among treatments, except for Expt 2, where they were significantly higher in the Fe+C than in the Fe treatment.

The P_{max} values, which were not normalized with Chl-*a* biomass, were positively correlated with the diatom-specific *rbcL* cDNA concentrations in all of the

experiments. The slopes of the regression lines were similar in Expts 1, 2, and 3, and the overall regression of these experiments exhibited a high determination coefficient ($r^2 = 0.929$, $p < 0.01$) (Fig. 6a). The slope of the regression line in Expt 4 was lower than that in the other experiments, although the correlation coefficient was the highest among the experiments ($r^2 = 0.977$, $p < 0.01$) (Fig. 6b).

Discussion

Hydrographic features and initial phytoplankton community composition

At all of the sampling stations, the surface seawater Chl-a concentrations were relatively low (0.26–0.62 µg L^{-1}), while nitrate remained >10 µmol L^{-1} (Table 1). The initial TDFe concentrations were also well below the values required for diatom growth (<0.35 nM; Sarthou et al. 2005), except in Expt 1. These results suggest that the initial seawater used in Expts 2, 3, and 4 represented HNLC conditions. However, the initial silicate concentration was depleted to below the half-saturation constants for diatom uptake (<3.9 µM; Sarthou et al. 2005) in Expt 1. The Expt 1 sampling site was located in the SAZ, where diatom biomass is thought to be limited by both Fe and silicate availability (i.e., an HNLSiLC regime; Boyd et al. 1999; Hutchins et al. 2001). In our observations, however, the TDFe concentration was relatively high compared with that of silicate (Table 1), suggesting that silicate was the more important limiting nutrient for diatom growth at that sampling site. Additionally, the Fe concentration (0.851 nM) value was nearly consistent with that reported in previous studies in the SAZ (Sedwick et al. 2008; Bowie et al. 2009). These studies suggested that the high Fe concentration in the SAZ is mainly caused by atmospheric dust deposition and advection of subtropical waters from the north. Although we did not evaluate other factors that could influence phytoplankton growth and primary productivity, such as grazing pressure, these results strongly indicate that phytoplankton biomass was controlled by micro- and/or macronutrient availability (i.e., bottom-up control) at the study sites.

Surface Chl-a concentrations and community compositions in the initial phytoplankton assemblages at each location were close to values previously observed in the same region in the summers of 1999–2000 (Ishikawa et al. 2002) and 2010–2011 (Takao et al. 2014). Based on the CHEMTAX analysis, we found a clear latitudinal gradient in the dominant phytoplankton taxa from haptophytes to diatoms (Fig. 3), which is likely related to the differences in silicate availability at each location; That is, the initial

silicate concentration decreased northward and was almost depleted in the northernmost station (Table 1). Additionally, as discussed above, there were severe Fe limitations in the initial Expt 2–4 samples. Our results suggest that Si availability can be an important factor controlling phytoplankton community composition, while Fe availability was the primary determinant of phytoplankton biomass.

Takao et al. (2014) showed that phytoplankton photosynthetic physiology, such as P_{max}^B and α^B, differs among Southern Ocean regions, with the values being higher in diatom-dominated than other areas. However, the P_{max}^B and α^B values observed in this study were insensitive to the dominant phytoplankton groups (Table 6).

Microscopic observation provided more detailed taxonomic information about the phytoplankton assemblages (Table 5; Hattori et al. in prep.). The major diatom species differed among geographical locations; F. kerguelensis and Chaetoceros sp. were predominant at the AZ and SPZ stations, respectively. F. kerguelensis makes significant contributions to the food web and carbon export to the deep sea in the study area (Perissinotto et al. 1997; Rigual-Hernández et al. 2016). Thalassiosira oestrupii initially dominated the diatom community at the SAZ station, where the silicate concentration was extremely low. Similarly, De Salas et al. (2011) also reported that weakly silicified Thalassiosira sp. dominated among diatoms in the Australian sector of the SAZ, suggesting that such centric diatom taxa may be favored by the low silicate concentration in the SAZ during the austral summer.

In terms of cell abundance, P. antarctica was the predominant haptophyte species in the initial samples in all of the experiments, although the calcifying haptophyte species E. huxleyi was also present at all of the locations, except at station D07. Previous field observations reported north–south (43–65°S) shifts in the E. huxleyi morphotype from the heavily calcified type A to the weakly calcified type B/C in the Australian sector of the Southern Ocean during 2002–2006; this shift was possibly related to a decline in the calcite saturation state (Cubillos et al. 2007). Our microscopic data showed that the E. huxleyi morphotype B/C dominated even at the northernmost experimental site (i.e., station C02, 45°S) in 2011–2012, implying that type A had been replaced by type A/B during the previous decade.

In Expts 2–4, the CHEMTAX analysis indicated that diatoms dominated the phytoplankton assemblage in the initial samples, although the haptophyte P. antarctica outcompeted diatoms in terms of cell abundance. These results are not mutually exclusive because cell abundance does not necessarily correlate with Chl-a biomass; For example, Garibotti et al. (2003) reported that a change in phytoplankton pigment concentration was consistent with

that in phytoplankton carbon biomass, but not with that in cell abundance on the Western Antarctic Peninsula coast. Moreover, phytoplankton cell pigment composition varies widely among species (Zapata et al. 2004), and can change under different environmental conditions, such as light and nutrient availability (DiTullio et al. 2007; Laviale and Neveux 2011). Another possible cause of the difference in the relative contribution of diatoms and haptophytes might be underestimation of diatom cells; That is, weakly silicified diatoms might have been lost during the sputtering process in our experiment.

Effects of Fe and CO_2 enrichment on phytoplankton assemblage

Increased Fe availability stimulated increases in Chl-a, Fuco, and 19′-Hex in Expts 1, 2, and 3, suggesting that both diatom and haptophyte growth are limited by Fe availability over a large area of the Southern Ocean (Fig. 2). This result was supported by the SEM observations, which revealed a substantial increase in diatom and haptophyte cell abundances in the Fe treatments compared with the control treatments (Table 5). Many studies have examined the effects of Fe enrichment on Southern Ocean phytoplankton assemblages, consistently demonstrating a significant increase in phytoplankton biomass with Fe enrichment (e.g., Boyd and Abraham 2001; Coale et al. 2004; Lance et al. 2007). Coale et al. (2004) have shown that the increase in phytoplankton biomass was greater in high- than in low-silicate water in the Southern Ocean, likely the result of preferential increase in diatoms with increased Fe availability. In our study, Fe-induced phytoplankton growth was also enhanced at the diatom-dominated locations in the AZ, where silicate availability was relatively high (Fig. 2b; Table 1).

The Fe-mediated shift in phytoplankton community composition was most pronounced at the northernmost station in the SAZ, where the noncalcifying haptophyte *P. antarctica* dominated the total phytoplankton population (Fig. 4b; Table 5). This was most likely because of the increases in the relative contributions of diatoms and calcifying haptophytes. The results of a metatranscriptomic study suggested that Fe enrichment could increase transcriptional activity in diatom genes related to silica transport and precipitation (Marchetti et al. 2012). Hence, one possible cause of the increase in diatom contribution in Expt 1 is that the Fe enrichment enabled diatoms to increase their silicate utilization efficiency by altering silicate metabolism.

The initial F_v/F_m values were consistently low at all of the sampling locations, and increased significantly with Fe enrichment in all of the experiments. This result suggests that PSII function was partly inhibited by low Fe availability in the study area. Our results are consistent with those previously reported by Boyd and Abraham (2001), who demonstrated a significant increase in F_v/F_m from ∼0.2 to ∼0.4 in response to Fe enrichment during an in situ Fe fertilization experiment in the Southern Ocean. Substantial increases in P_{max}^B and α^B were also observed under Fe-enriched conditions in the experiments conducted in the SAZ and AZ. These results strongly indicate that Fe availability was an important factor influencing the phytoplankton photosynthesis efficiency in both light and dark reactions in the study area. Moreover, these increases in photosynthetic performance were likely associated with the increases in Chl-a biomass in the Fe treatments.

Despite the large variations in P_{max}^B and α^B, the E_k values remained relatively constant between the Fe-limited and Fe-replete conditions in all of the experiments (Table 6). This phenomenon is referred to as E_k-independent variability (Behrenfeld et al. 2004), and our result is consistent with that previously reported from an in situ Fe fertilization experiment (Gervais et al. 2002) and a laboratory experiment (Davey and Geider 2001). E_k-independent variability can be driven by shifts in cellular energy allocation (Behrenfeld et al. 2008; Halsey and Jones 2015). Furthermore, the increase in P_{max} was accompanied by an increase in diatom-specific *rbcL* gene transcript abundance, and consequently, significant correlations were found between these photosynthetic parameters (Fig. 6). Similar results have been obtained in North America (Corredor et al. 2004; John et al. 2007).

Notably, Fe had no significant effect on either Chl-a or Fuco in Expt 4, despite the low ambient TDFe concentration. This result indicates that Fe availability was not a primary factor affecting phytoplankton growth at that sampling site. However, the F_v/F_m response suggests that the photosynthetic capacity in the community would be limited by low Fe concentration, at least in terms of the photochemical quantum efficiency of PSII. After incubation, the Chl-a concentration in the control treatment increased compared with the Fe treatment in Expt 4, indicating that some unknown factor triggered abrupt phytoplankton growth, primarily in diatoms. One of our study sites was located in the Antarctic marginal ice zone (MIZ), where phytoplankton blooms can occur in spring and early summer (Arrigo et al. 1999; Smetacek et al. 2004; Davidson et al. 2010). However, taxonomic composition varies among locations, possibly because of differences in environmental conditions; For example, diatoms tend to dominate in highly stratified water columns, whereas the colonial haptophyte *P. antarctica* can dominate in deeply mixed water columns in the Southern Ocean (Arrigo et al. 1999; Mills et al. 2010), although

contrasting results have also been reported (Kang et al. 2001). Moreover, diatoms would have a competitive advantage over *P. antarctica* under constant and high light conditions (Arrigo et al. 2010). In our experiments, the so-called bottle effect (i.e., artifacts produced by bottle incubation) might have affected phytoplankton assemblage growth dynamics. Furthermore, bottle incubation alters the physical seawater conditions, such as light intensity and mixing, which may have made them more favorable for diatom than haptophyte growth. Although other factors, such as selective grazing, have also been proposed to explain phytoplankton community formation, the mechanisms governing the onset and taxonomic composition of phytoplankton blooms in the study area remain unknown (Lancelot et al. 1993; van Hilst and Smith 2002; Smetacek et al. 2004). Further study is needed to gain a better understanding of the particular biological responses to Fe enrichment in Expt 4.

Under Fe-replete conditions, we discovered that CO_2 availability led to a decrease in the diatom marker in Expt 3 (Fig. 2b). Additionally, the haptophyte marker decreased in Expts 1 and 2 (Fig. 2c). SEM also detected decreases in both diatom and haptophyte markers, although the magnitude differed between pigment concentration and cell abundance (Table 5). Our results are consistent with previous laboratory culture experiments, which demonstrated significant decreases in growth rate and/or Chl-*a* content in two major Antarctic phytoplankton taxa, the diatom *F. cylindrus* and the haptophyte *P. antarctica*, in response to increased CO_2 levels under Fe-replete conditions (Xu et al. 2014). From a field incubation experiment conducted in the Ross Sea, Feng et al. (2010) were first to demonstrate that elevated CO_2 levels lead to a decrease in *P. antarctica* growth in the Southern Ocean, specifically in low-light conditions. There is also some evidence that high CO_2 levels can alter the abundance and community composition of the natural Southern Ocean diatom community, although responses have not been consistent among experiments (Tortell et al. 2008; Feng et al. 2010; Hoppe et al. 2013; Maas et al. 2013).

Our study also revealed a strong geographical difference in phytoplankton responses to changes in CO_2 availability under Fe-enriched conditions, and this was probably related to the community composition (Figs. 4a, c). Despite significant changes in phytoplankton pigment signature, the impacts of elevated CO_2 levels on the shift in overall phytoplankton community were small in Expts 2, 3, and 4 (Fig. 4c). Contrastingly, the phytoplankton community shifted significantly under high-CO_2 conditions in Expt 1, likely because of the selective decrease in calcifying haptophytes (Figs. 3, 4c). According to the microscopy data, dominant coccolithophore (*Calcidiscus leptopus* and

E. huxleyi) cell abundance decreased in the high-CO_2 treatments (Hattori et al. in prep). This was most likely caused by a decrease in the seawater calcium carbonate ($CaCO_3$) saturation state, which likely has adverse impact on coccolithophore calcification (Riebesell et al. 2000; Müller et al. 2010). According to Cubillos et al. (2007), the seawater $CaCO_3$ saturation state can control *E. huxleyi* calcification and distribution in the Southern Ocean. A decrease in coccolithophore abundance may provide a negative feedback to OA, because the calcification process increases seawater CO_2 concentrations by reducing TA (Gehlen et al. 2011). However, it is difficult to explore a single feedback process to predict future OA impacts because of the complex role that coccolithophores play in marine biogeochemical cycles; For example, because $CaCO_3$ can increase settling aggregate sinking velocity, *E. huxleyi* might contribute to the biological carbon pump in the study area (Iversen and Ploug 2010).

Increased CO_2 availability rarely affected the photosynthetic parameters in any of the experiments (Fig. 5). In terms of F_v/F_m, our results were similar to those in the western North Pacific (Endo et al. 2013, 2016), the Bering Sea (Sugie et al. 2013), and the Southern Ocean (Hoppe et al. 2013; Coad et al. 2016). These studies all reported that increased CO_2 levels had no effect on the maximum quantum efficiency of PSII photochemistry. In contrast, the light-independent cycle of photosynthesis (i.e., the Calvin cycle) might be more sensitive to changes in CO_2 availability. Some field studies have reported downregulation of either the key carbon fixation enzyme RuBisCO or its encoding gene *rbcL* in response to increased CO_2 levels (Losh et al. 2013; Endo et al. 2015). However, the present study did not find any evidence of reduced diatom-specific *rbcL* transcriptional activity in response to elevated CO_2 concentrations. Because the sensitivity of *rbcL* transcription to changing CO_2 conditions can differ greatly among diatom taxa (Endo et al. 2016), the discrepancy in photosynthetic physiological responses among experiments might have been the result of differences in phytoplankton species composition. Additionally, other environmental factors, such as micro- and/or macronutrient concentrations, can modulate the CO_2-related changes in RuBisCO activity (John et al. 2010).

As with the other photosynthetic parameters, the phytoplankton assemblage Chl-*a* normalized maximum photosynthetic rate (P_{max}^B) did not change significantly among different CO_2 levels, although it increased slightly in Expts 1 and 3 (Fig. 5c). Elevated CO_2 levels tend to increase the algal carbon fixation rate at the single culture level, although the extent varies widely among phytoplankton species depending on their physiological mechanisms (Burkhardt et al. 2001; Trimborn et al. 2009). However,

significant increases in maximum carbon fixation rate and/ or cell growth have rarely been observed at community level (Delille et al. 2005; Hare et al. 2007; Feng et al. 2009). Possible explanations for this discrepancy are species interactions, such as competitive exclusion and allelopathic effects (Trimborn et al. 2013). Because biotic interactions are difficult to predict from theoretical studies and laboratory culture experiments, further field observations are necessary to interpret the differences observed.

The present study is the first to investigate the impacts of CO_2 enrichment on a phytoplankton community in four different geographical locations in the Australian sector of the Southern Ocean. Increased CO_2 levels had little effect on phytoplankton biomass, community composition, and photosynthetic capacity in the AZ and SPZ, although they significantly altered community composition in the SAZ. The geographical dependence of phytoplankton responses to increased CO_2 levels was likely caused by the negative effect observed on coccolithophores. Our results suggest that the impacts of OA on the Southern Ocean phytoplankton community would be most pronounced in the haptophyte-dominated SAZ. This region may be particularly important in the Southern Ocean within the context of the carbon cycle and ecosystem functioning because the SAZ accounts for ∼50% of the open Southern Ocean (Boyd et al. 1999) and is a major contributor to global primary productivity (Banse 1996; McNeil et al. 2007; Takahashi et al. 2009). Therefore, a future increase in CO_2 might alter the food web structure and biogeochemical cycles in this region.

Because we did not assess the effects of elevated CO_2 under ambient Fe conditions, our results need to be verified when OA coincides with Fe enrichment in the study area. Moreover, because of the small number of treatment replicates and the short incubation times, our study might have failed to capture some significant responses. Additionally, other climate-mediated changes, such as ocean warming and increased iceberg fluxes, may alter the magnitude and timing of nutrient pulses in the AZ and SPZ (Timmermann and Hellmer 2013; Duprat et al. 2016). Further work on the combined effects of OA and other stressors is required to better understand the potential impact of OA in the Southern Ocean.

Compliance with ethical standards

Conflict of interest The authors declare that they have no conflict of interest.

Ethical approval This article does not contain any studies with human participants or animals performed by any of the authors. All procedures performed were in accordance with the ethical standards of the Hokkaido University.

References

Arrigo KR, Robinson DH, Worthen DL, Dunbar RB, DiTullio GR, VanWoert M, Lizotte MP (1999) Phytoplankton community structure and the drawdown of nutrients and CO_2 in the Southern Ocean. Science 283:365–367

Arrigo KR, van Dijken GL, Bushinsky S (2008) Primary production in the Southern Ocean, 1997–2006. J Geophys Res. doi:10.1029/2007JC004551

Arrigo KR, Mills MM, Kropuenske LR, van Dijken GL, Alderkamp AC, Robinson DH (2010) Photophysiology in two major Southern Ocean phytoplankton taxa: photosynthesis and growth of *Phaeocystis antarctica* and *Fragilariopsis cylindrus* under different irradiance levels. Integr Comp Biol 50:950–966

Banse K (1996) Low seasonality of low concentrations of surface chlorophyll in the Subantarctic water ring: underwater irradiance, iron, or grazing? Prog Oceanogr 37:241–291

Bednaršek N, Tarling GA, Bakker DCE, Fielding S, Jones EM, Venables HJ, Ward P, Luzirian A, Lézé B, Murphy EJ (2012) Extensive dissolution of live pteropods in the Southern Ocean. Nat Geosci 5:881–885

Behrenfeld MJ, Prasil O, Babin M, Bruyant F (2004) In search of a physiological basis for covariations in light-limited and light-saturated photosynthesis. J Phycol 40:4–25

Behrenfeld MJ, Halsey KH, Milligan AJ (2008) Evolved physiological responses of phytoplankton to their integrated growth environment. Philos Trans R Soc B 363:2687–2703

Bowie AR, Lannuzel D, Remenyi TA, Wagener T, Lam PJ, Boyd PW, Guieu C, Townsend AT, Trull TW (2009) Biogeochemical iron budgets of the Southern Ocean south of Australia: decoupling of iron and nutrient cycles in the subantarctic zone by the summertime supply. Glob Biogeochem Cy. doi:10.1029/2009GB003500

Boyd PW, Abraham ER (2001) Iron-mediated changes in phytoplankton photosynthetic competence during SOIREE. Deep Sea Res II 48:2529–2550

Boyd PW, LaRoche J, Gall M, Frew R, McKay RML (1999) The role of iron, light and silicate in controlling algal biomass in sub-Antarctic waters SE of New Zealand. J Geophys Res 104:13395–13408

Boyd PW, Arrigo KR, Strzepek R, Dijken GL (2012) Mapping phytoplankton iron utilization: insights into Southern Ocean supply mechanisms. J Geophys Res. doi:10.1029/2011JC007726

Burkhardt S, Amoroso G, Riebesell U, Sültemeyer D (2001) CO_2 and HCO_3^- uptake in marine diatoms acclimated to different CO_2 concentrations. Limnol Oceanogr 46:1378–1391

Caldeira K, Wickett ME (2003) Oceanography: anthropogenic carbon and ocean pH. Nature 425:365

Coad T, McMinn A, Nomura D, Martin A (2016) Effect of elevated CO_2 concentration on microalgal communities in Antarctic pack ice. Deep Sea Res II 131:160–169

Coale KH, Johnson KS, Chavez FP, Buesseler KO, Barber RT, Brzezinski MA, Cochlan WP, Millero FJ, Falkowski PG, Bauer JE, Wanninkhof RH, Kudela RM, Altabet MA, Hales BE, Takahashi T, Landry MR, Bidigare RR, Wang XJ, Chase Z, Strutton PG, Friederich GE, Gorbunov MY, Lance VP, Hilting AK, Hiscock MR, Demarest M, Hiscock WT, Sullivan KF, Tanner SJ, Gordon RM, Hunter CN, Elrod VA, Fitzwater SE, Jones JL, Tozzi S, Koblizek M, Roberts AE, Herndon J, Brewster J, Ladizinsky N, Smith G, Cooper D, Timothy D, Brown SL, Selph KE, Sheridan CC, Twining BS, Johnson ZI (2004) Southern ocean iron enrichment experiment: carbon cycling in high- and low-Si waters. Science 304:408–414

Comeau S, Gorsky G, Jeffree R, Teyssié J-L, Gattuso J-P (2009) Impact of ocean acidification on a key Arctic pelagic mollusk (*Limacina helicina*). Biogeosciences 6:1877–1882

Corredor JE, Wawrik B, Paul JH, Tran H, Kerkhof L, Lopez JM, Dieppa A, Cardenas O (2004) Geochemical rate-RNA integrated study: ribulose-1,5-bisphosphate carboxylase/oxygenase gene transcription and photosynthetic capacity of planktonic photoautotrophs. Appl Environ Microbiol 70:5459–5468

Cubillos JC, Wright SW, Nash G, de Salas MF, Griffiths B, Tilbrook B, Poisson A, Hallegraeff GM (2007) Shifts in geographic distribution of calcification morphotypes of the coccolithophorid *Emiliania huxleyi* in the Australian sector of the Southern Ocean during 2001–2006. Mar Ecol Prog Ser 348:47–54

Davey M, Geider RJ (2001) Impact of iron limitation on the photosynthetic apparatus of the diatom *Chaetoceros muelleri* (Bacillariophyceae). J Phycol 37:987–1000

Davidson AT, Scott FJ, Nash GV, Wright SW, Raymond B (2010) Physical and biological control of protistan community composition, distribution and abundance in the seasonal ice zone of the Southern Ocean between 30 and 80°E. Deep Sea Res II 57:828–848

de Baar HJW, de Jong JTM, Bakker DCE, Löscher BM, Veth C, Bathmann U, Smetacek V (1995) Importance of iron for plankton blooms and carbon dioxide drawdown in the Southern Ocean. Nature 373:412–415

de Salas MF, Eriksen R, Davidson AT, Wright SW (2011) Protistan communities in the Australian sector of the Sub-Antarctic Zone during SAZ-Sense. Deep Sea Res II 58:2135–2149

Delille B, Harlay J, Zondervan I, Jacquet S, Chou L, Wollast R, Bellerby RGJ, Frankignoulle M, Borges AV, Riebesell U, Gattuso J-P (2005) Responses of primary production and calcification to changes of pCO_2 during experimental blooms of the coccolithophorid *Emiliania huxleyi*. Glob Biogeochem Cycle. doi:10.1029/B002318

DiTullio GR, Garcia N, Riseman SF, Sedwick PN (2007) Effects of iron concentration on pigment composition in *Phaeocystis antarctica* grown at low irradiance. Biogeochemistry 83:71–81

Duprat LP, Bigg GR, Wilton DJ (2016) Enhanced Southern Ocean marine productivity due to fertilization by giant icebergs. Nat Geosci 9:219–221

Edmond JM (1970) High precision determination of titration alkalinity and total carbon dioxide content of sea water by potentiometric titration. Deep Sea Res 17:737–750

Endo H, Yoshimura T, Kataoka T, Suzuki K (2013) Effects of CO_2 and iron availability on phytoplankton and eubacterial community compositions in the northwest subarctic Pacific. J Exp Mar Biol Ecol 439:160–175

Endo H, Sugie K, Yoshimura T, Suzuki K (2015) Effects of CO_2 and iron availability on *rbcL* gene expression in Bering Sea diatoms. Biogeosciences 12:2247–2259

Endo H, Sugie K, Yoshimura T, Suzuki K (2016) Response of spring diatoms to CO_2 availability in the western North Pacific as determined by next-generation sequencing. PLoS ONE 11:e0154291. doi:10.1371/journal.pone.0154291

Feng YY, Hare CE, Leblance K, Rose JM, Zhang YH, DiTullio GR, Lee PA, Whlhelm SW, Rowe JM, Sun J, Nemcek N, Gueguen C, Passow U, Benner I, Brown C, Hutchins DA (2009) Effects of increased pCO_2 and temperature on the North Atlantic spring bloom. I. The phytoplankton community and biogeochemical response. Mar Ecol Prog Ser 388:13–25

Feng Y, Hare CE, Rose JM, Handy SM, DiTullio GR, Lee PA, Smith WO, Peloquin J, Tozzi S, Sun J, Zhang Y, Dunbar RB, Long MC, Sohst B, Lohan M, Hutchins DA (2010) Interactive effects of iron, irradiance and CO_2 on Ross Sea phytoplankton. Deep Sea Res Part I 57:368–383

Freeman NM, Lovenduski NS (2015) Decreased calcification in the Southern Ocean over the satellite record. Geophys Res Lett 42:1834–1840

Garibotti IA, Vernet M, Kozlowski WA, Ferrario ME (2003) Composition and biomass of phytoplankton assemblages in coastal Antarctic waters: a comparison of chemotaxonomic and microscopic analyses. Mar Ecol Prog Ser 247:27–42

Gehlen M, Gruber N, Gangstø R, Bopp L, Oschlies A (2011) Biogeochemical consequences of ocean acidification and feedbacks to the earth system. In: Gattuso J-P, Hansson L (eds) ocean acidification. Oxford University Press, New York, pp 230–248

Gervais F, Riebesell U, Gorbunov MY (2002) Changes in primary productivity and chlorophyll a in response to iron fertilization in the Southern Polar Frontal Zone. Limnol Oceanogr 47:1324–1335

Halsey KH, Jones BM (2015) Phytoplankton strategies for photosynthetic energy allocation. Annu Rev Mar Sci 7:265–297

Hama T, Miyazaki T, Ogawa Y, Iwakuma T, Takahashi M, Otsuki A, Ichimura S (1983) Measurement of photosynthetic production of a marine phytoplankton population using a stable ^{13}C isotope. Mar Biol 73:31–36

Hare CN, Leblanc K, DiTullio GR, Kudela RM, Zhang Y, Lee PA, Riseman S, Hutchins DA (2007) Consequences of increased temperature and CO_2 for phytoplankton community structure in the Bering Sea. Mar Ecol Prog Ser 352:9–16

Hoppe CJ, Hassler CS, Payne CD, Tortell PD, Rost B, Trimborn S (2013) Iron limitation modulates ocean acidification effects on Southern Ocean phytoplankton communities. PLoS ONE 8:e79890. doi:10.1371/journal.pone.0079890

Huntley ME, Lopez MDG, Karl DM (1991) Top predators in the Southern Ocean: a major leak in the biological carbon pump. Science 253:64–66

Hutchins DA, Boyd PW (2016) Marine phytoplankton and the changing ocean iron cycle. Nat Clim Chang 6:1072–1079

Hutchins DA, Sedwick PN, DiTullio GR, Boyd PW, Quéguiner B, Griffiths FB, Crossley C (2001) Control of phytoplankton growth by iron and silicic acid availability in the subantarctic Southern Ocean: experimental results from the SAZ project. J Geophys Res 106:559–572

Isada T, Kuwata A, Saito H, Ono T, Ishii M, Yoshikawa-Inoue H, Suzuki K (2009) Photosynthetic features and primary productivity of phytoplankton in the Oyashio and Kuroshio-Oyashio transition regions of the northwest Pacific. J Plankton Res 31:1009–1025

Ishikawa A, Wright SW, van den Enden R, Davidson AT, Marchant HJ (2002) Abundance, size structure and community composition of phytoplankton in the Southern Ocean in the austral summer 1999/2000. Polar Biosci 15:11–26

Iversen MH, Ploug H (2010) Ballast minerals and the sinking carbon flux in the ocean: carbon-specific respiration rates and sinking velocity of marine snow aggregates. Biogeosciences 7:2613–2624

Jeffrey SW, Vesk M (1997) Introduction to marine phytoplankton and their pigment signatures. In: Jeffrey SE, Mantoura RFC, Wright SW (eds) Phytoplankton pigments in oceanography: guidelines to modern methods. UNESCO Publishing, Paris, pp 37–84

Jeffrey SW, Wright SW (1994) Photosynthetic pigments in the Haptophyta. In: Leadbeater BSC (ed) The haptophyte algae. Clarendon, Oxford, pp 111–132

John DE, Wang ZA, Liu XW, Byrne RH, Corredor JE, Lopez JM, Cabrera A, Bronk DA, Tabita FR, Paul JH (2007) Phytoplankton carbon fixation gene (RuBisCO) transcripts and air-sea CO_2 flux in the Mississippi River plume. ISME J 1:517–531

John DE, Jose López-Díaz JM, Cabrera A, Santiago NA, Corredor JE, Bronk DA, Paul JH (2010) A day in the life in the dynamic marine environment: how nutrients shape diel patterns of phytoplankton photosynthesis and carbon fixation gene expression in the Mississippi and Orinoco river plumes. Hydrobiologia 679:155–173

Kang SH, Kang JS, Lee S, Chung KH, Kim D, Park MG (2001) Antarctic phytoplankton assemblages in the marginal ice zone of the northwestern Weddell Sea. J Plankton Res 23:333–352

Khatiwala S, Primeau F, Hall T (2009) Reconstruction of the history of anthropogenic CO_2 concentrations in the ocean. Nature 462:346–349

Lance VP, Hiscock MR, Hilting AK, Stuebe DA, Bidigare RR, Smith WO, Barber RT (2007) Primary productivity, differential size fraction and pigment composition responses in two Southern Ocean in situ iron enrichments. Deep Sea Res Part I 54:747–773

Lancelot C, Mathot S, Veth C, de Baar H (1993) Factors controlling phytoplankton ice-edge blooms in the marginal ice-zone of the northwestern Weddell Sea during sea ice retreat 1988: field observations and mathematical modelling. Polar Biol 13:377–387

Latasa M (2007) Improving estimations of phytoplankton class abundances using CHEMTAX. Mar Ecol Prog Ser 329:13–21

Laviale M, Neveux J (2011) Relationships between pigment ratios and growth irradiance in 11 marine phytoplankton species. Mar Ecol Prog Ser 425:63–77

Longhurst A (2007) Ecological geography of the sea, 2nd edn. Academic, Burlington

Losh JL, Young JN, Morel FM (2013) Rubisco is a small fraction of total protein in marine phytoplankton. New Phytol 198:52–58

Maas EW, Law CS, Hall JA, Pickmere S, Currie KI, Chang FH, Voyles KM, Caird D (2013) Effect of ocean acidification on bacterial abundance, activity and diversity in the Ross Sea, Antarctica. Aquat Microb Ecol 70:1–15

Malinverno E, Maffioli P, Gariboldi K (2016) Latitudinal distribution of extant fossilizable phytoplankton in the Southern Ocean: planktonic provinces, hydrographic fronts and palaeoecological perspectives. Mar Micropaleontol 123:41–58

Marchetti A, Schruth DM, Durkin CA, Parker MS, Kodner RB, Berthiaume CT, Morales R, Allen AE, Armbrust EV (2012) Comparative metatranscriptomics identifies molecular bases for the physiological responses of phytoplankton to varying iron availability. Proc Natl Acad Sci USA 109:E317–E325

Martin JH, Gordon RM, Fitzwaters SE (1990) Iron in Antarctic waters. Nature 345:156–158

Marx FG, Uhen MD (2010) Climate, critters, and cetaceans: cenozoic drivers of the evolution of modern whales. Science 327:993–996

McNeil BI, Metzl N, Key RM, Matear RJ, Corbiere A (2007) An empirical estimate of the Southern Ocean air–sea CO_2 flux. Glob Biogeochem Cycle. doi:10.1029/2007GB002991

Mills MM, Kropuenske LR, Van Dijken GL, Alderkamp AC, Berg GM, Robinson DH, Welschmeyer NA, Arrigo KR (2010) Photophysiology in two Southern Ocean phytoplankton taxa: photosynthesis of *Phaeocystis antarctica* (Prymnesiophceae) and *Fragilariopsis cylindrus* (Bacillariophyceae) under simulated in situ mixed-layer irradiance. J Phycol 46:1114–1127

Moy AD, Howard WR, Bray SG, Trull TW (2009) Reduced calcification in modern Southern Ocean planktonic foraminifera. Nat Geosci 2:276–280

Müller M, Schulz K, Riebesell U (2010) Effects of long-term high CO_2 exposure on two species of coccolithophores. Biogeosciences 7:1109–1116

NOAA (2016) Trends in atmospheric carbon dioxide. http://www.esrl.noaa.gov/gmd/ccgg/trends/global.html. Accessed 20 July 2016

Obata H, Karatani H, Matsui M, Nakayama E (1997) Fundamental studies for chemical speciation of iron in seawater with an improved analytical method. Mar Chem 56:97–106

Ondrusek ME, Bidigare RR, Sweet ST, Defreitas DA, Brooks JM (1991) Distribution of phytoplankton pigments in the North Pacific Ocean in relation to physical and optical variability. Deep Sea Res 38:243–266

Orr JC, Fabry VJ, Aumont O, Bopp L, Doney SC, Feely RA, Gnanadesikan A, Gruber N, Ishida A, Joos F, Key RM, Lindsay K, Maier-Reimer E, Matear R, Monfray P, Mouchet A, Najjar RG, Plattner G-K, Rodgers KB, Sabine CL, Sarmiento JL, Schlitzer R, Slater RD, Totterdell IJ, Weirig M-F, Yamanaka Y, Yool A (2005) Anthropogenic ocean acidification over the twenty-first century and its impact on calcifying organisms. Nature 437:681–686

Orsi AH, Whitworth T III, Nowlin WD (1995) On the meridional extent and fronts of the Antarctic Circumpolar Current. Deep Sea Res I 42:641–673

Perissinotto R, Pakhomov EA, McQuaid CD, Froneman PW (1997) In situ grazing rates and daily ration of Antarctic krill *Euphausia superba* feeding on phytoplankton at the Antarctic Polar Front and the Marginal Ice Zone. Mar Ecol Prog Ser 160:77–91

Pierrot D, Lewis E, Wallace DWR (2006) MS Excel program developed for CO_2 system calculations. ORLN/CDIAC-105, Carbon Dioxide Information Analysis Center, Oak Ridge National Laboratory, US Department of Energy, Oak Ridge

Platt T, Gallegos CL, Harrison WG (1980) Photoinhibition of photosynthesis in natural assemblages of marine phytoplankton. J Mar Res 38:687–701

Riebesell U, Zondervan I, Rost B, Tortell PD, Zeebe RE, Morel FMM (2000) Reduced calcification of marine plankton in response to increased atmospheric CO_2. Nature 407:364–367

Rigual-Hernández AS, Trull TW, Bray SG, Armand LK (2016) The fate of diatom valves in the Subantarctic and Polar Frontal Zones of the Southern Ocean: sediment trap versus surface sediment assemblages. Palaeogeogr Palaeocl 457:129–143

Sarthou G, Timmermans KR, Blain S, Treguer P (2005) Growth physiology and fate of diatoms in the ocean: a review. J Sea Res 53:25–42

Scott FJ, Thomas DP (2005) Diatoms. In: Scott FJ, Marchant HJ (eds) Antarctic marine protists. Australian Biological Resources Study, Canberra, pp 13–201

Sedwick PN, Bowie AR, Trull TW (2008) Dissolved iron in the Australian sector of the Southern Ocean (CLIVAR SR3 section): meridional and seasonal trends. Deep Sea Res Part I 55:911–925

Smetacek V, Assmy P, Henjes J (2004) The role of grazing in structuring Southern Ocean pelagic ecosystems and biogeochemical cycles. Antarct Sci 16:541–558

Speer K, Rintoul SR, Sloyan B (2000) The diabatic deacon cell. J Phys Oceanogr 30:3212–3222

Sugie K, Endo H, Suzuki K, Nishioka J, Kiyosawa H, Yoshimura T (2013) Synergistic effects of pCO_2 and iron availability on nutrient consumption ratio of the Bering Sea phytoplankton community. Biogeosciences 10:6309–6321

Takahashi T, Sutherland SC, Wanninkhof R, Sweeney C, Feely RA, Chipman D, Hales B, Friederich G, Chavez F, Watson A, Bakker D, Schuster U, Metzl N, Inoue HY, Ishii M, Midorikawa T, Sabine C, Hoppema M, Olafsson J, Amarson T, Tilbrook B, Johannessen T, Olsen A, Bellerby R, DeBaar H, Nojiri Y, Wong CS, Delille B, Bates NR, de Baar HJW (2009) Climatological mean and decadal change in surface ocean pCO_2, and net sea-air CO_2 flux over the global oceans. Deep Sea Res Part II 56:554–577

Takahashi T, Sweeney C, Hales B, Chipman DW, Newberger T, Goddard JG, Iannuzzi RA, Sutherland SC (2012) The changing carbon cycle in the Southern Ocean. Oceanography 25:26–37

Takao S, Hirawake T, Hashida G, Sasaki H, Hattori H, Suzuki K (2014) Phytoplankton community composition and photosynthetic physiology in the Australian sector of the Southern Ocean during the austral summer of 2010/2011. Polar Biol 37:1563–1578

Takeda S, Obata H (1995) Response of equatorial Pacific phytoplankton to subnanomolar Fe enrichment. Mar Chem 50:219–227

Thomas CR (1997) Identifying marine phytoplankton. Academic Press, San Diego

Timmermann R, Hellmer HH (2013) Southern Ocean warming and increased ice shelf basal melting in the twenty-first and twenty-second centuries based on coupled ice-ocean finite-element modelling. Ocean Dyn 63:1011–1026

Tortell PD, Payne CD, Li Y, Trimborn S, Rost B, Smith WO, Riesselman C, Dunbar RB, Sedwick P, DiTullio GR (2008) CO_2 sensitivity of Southern Ocean phytoplankton. Geophys Res Lett. doi:10.1029/2007GL032583

Trimborn S, Wolf-Gladrow D, Richter KU, Rost B (2009) The effect of pCO_2 on carbon acquisition and intracellular assimilation in four marine diatoms. J Exp Mar Biol Ecol 376:26–36

Trimborn S, Brenneis T, Sweet E, Rost B (2013) Sensitivity of Antarctic phytoplankton species to ocean acidification: growth, carbon acquisition, and species interaction. Limnol Oceanogr 58:997–1007

Trimborn S, Thoms S, Petrou K, Kranz SA, Rost B (2014) Photophysiological responses of Southern Ocean phytoplankton to changes in CO_2 concentrations: short-term versus acclimation effects. J Exp Mar Biol Ecol 451:44–54

van Hilst CM, Smith WO (2002) Photosynthesis/irradiance relationships in the Ross Sea, Antarctica, and their control by phytoplankton assemblage composition and environmental factors. Mar Ecol Prog Ser 226:1–12

Woodward S, Roberts DL, Betts RA (2005) A simulation of the effect of climate change-induced desertification on mineral dust aerosol. Geophys Res Lett. doi:10.1029/2005GL02348

Wright SW, van den Enden RL (2000) Phytoplankton community structure and stocks in the east Antarctic marginal ice zone (BROKE survey, January–March 1996) determined by CHEM-TAX analysis of HPLC pigment signature. Deep Sea Res Part II 47:2363–2400

Xu K, Fu FX, Hutchins DA (2014) Comparative responses of two dominant Antarctic phytoplankton taxa to interactions between ocean acidification, warming, irradiance, and iron availability. Limnol Oceanogr 59:1919–1931

Young JR, Geisen M, Cros L, Kleijne A, Sprengel C, Probert I, Østergaard JB (2003) A guide to extant coccolithophore taxonomy. J Nanoplankton Res Spec Issue 1:1–124

Zapata M, Jeffrey SW, Wright SW, Rodríguez F, Garrido JL, Clementson L (2004) Photosynthetic pigments in 37 species (65 strains) of Haptophyta: implications for oceanography and chemotaxonomy. Mar Ecol Prog Ser 270:83–102